# Dynamic extension of the Keldysh-Rutherford model for attoclocks

Vladislav V. Serov [1,*] and Anatoli S. Kheifets [2]

[1]*Department of General, Theoretical and Computer Physics, Saratov State University, 83 Astrakhanskaya, Saratov 410012, Russia*

[2]*Research School of Physics, The Australian National University, Canberra ACT 2601, Australia*

(Received 24 October 2021; revised 30 January 2022; accepted 6 June 2022; published 17 June 2022)

The classical Keldysh-Rutherford (KR) model of the attoclock [A. W. Bray *et al.*, Phys. Rev. Lett. **121**, 123201 (2018)] was introduced to interpret attosecond angular streaking on atomic hydrogen in the low laser intensity regime. In this model, the photoelectron acquires its final velocity immediately after exiting the tunnel and then scatters elastically on the Coulomb field of the residual ion. In the present work, we make a dynamic extension of the KR model and consider a gradual acceleration of the photoelectron by the driving laser field. By doing so, we observe and explain a significant displacement of the peaks of the angular distribution of the mean photoelectron momentum and the angular resolved ionization probability. These peaks should be close within the original KR model.

DOI: 10.1103/PhysRevA.105.063106

## I. INTRODUCTION

Attosecond angular streaking (the attoclock) is a commonly used technique that explores the tunneling ionization of atoms and molecules in a strong laser field. The attoclock technique detects the position of the angular maximum of the photoelectron momentum distribution (PMD) in the polarization plane of a slightly elliptical laser pulse. The attoclock attempts to relate the offset angle $\theta_a$ of this maximum relative to the minor polarization axis with the time the tunneling electron spends under the barrier (the tunneling time) [1–4]. The photoelectron tunneling, as an exponentially suppressed process, occurs predominantly at the peak electric field strength of the driving laser pulse. At this instant, the electric field is aligned with the major axis of the polarization ellipse. The photoelectron emerges from the tunnel with a nearly zero velocity and its canonical momentum captures the vector potential of the laser field at the time of exit. This momentum is carried to the detector and its angular displacement relative to the minor polarization axis is converted to the tunneling time $\tau = \theta_a/\omega$, where $\omega$ is the angular frequency of the driving field. A similar attoclock reading $\theta_a$ can be obtained from numerical simulations with very short, nearly single oscillation, circularly polarized pulses. The latest attoclock experiments proved to be inconclusive as to whether the tunneling time is finite [5] or vanishing [6], and the debates are still being waged to resolve this issue [7–9].

An accurate theoretical description of the atomic attoclock is provided by a numerical solution of the time-dependent Schrödinger equation (TDSE). Such a solution is exact for the atomic hydrogen [10,11] and is restricted by the single active electron (SAE) approximation for noble gas atoms [12–15]. While the TDSE solution is numerically accurate, it is not particularly revealing for qualitative aspects of tunneling ionization. In particular, it does not reveal the time and velocity of the photoelectron when exiting the tunnel. So the most important questions as to a finite versus vanishing tunneling time and the adiabatic versus nonadiabatic tunneling cannot be easily resolved. To answer these questions, various analytic models were developed and calibrated against numerically accurate TDSE results. Thus validated models, in turn, revealed the photoelectron time and velocity at the exit from the tunnel and thus allowed the establishment of the tunneling time, as finite or vanishing. Several such analytic models were proposed. Among them are the tunnel ionization in parabolic coordinates with induced dipole and Stark shift (TIPIS) [3], the Wigner trajectory [16], the analytic $R$ matrix [10], the classical back-propagation [17], and the classical-trajectory Monte Carlo [18]. These models highlight various aspects of the tunneling process and the subsequent interaction of the ionized electron with the driving laser field on its way out towards the detector.

The classical Keldysh-Rutherford (KR) model [19] simplifies this interaction considerably. In the KR model, it is assumed that the photoelectron acquires its final velocity immediately after exiting the tunnel and then it scatters elastically on the Coulomb field of the ion remainder. The Rutherford scattering formula is applied with the impact parameter being replaced with the tunnel width provided by the Keldysh theory. The predictions of the KR model are numerically accurate in the very low laser field intensity regime. In addition, it correctly predicts the analytic dependence of the attoclock offset angle on the laser intensity, the carrier frequency, and the atomic ionization potential. However, the KR model fails for the modestly strong laser intensities that are commonly used in the experiment. This failure is related to the ongoing interaction of the photoelectron with the laser field that is ignored in the KR model. In reality, the photoelectron exits the tunnel with a nearly zero velocity and then is gradually accelerated to its final velocity by the laser pulse.

*vladislav_serov@mail.ru

 

In the present work, we remedy this deficiency of the KR model and develop its dynamic extension. In such an extended DKR model, the initial conditions for the electron after exiting the tunnel are taken from the Keldysh theory. With these initial conditions, the classical photoelectron trajectory is calculated by solving the Newton's equation of motion under the action of the laser pulse and the Coulomb field of the residual ion. Conceptually, the DKR approach is similar to the TIPIS model [3]. However, the latter model experiences some difficulties. Agreement of the TIPIS model with the experiment and the numerical TDSE solution was achieved only when the polarization of the residual ions was taken into account. Meanwhile, the TDSE solution did not include such a polarization, which therefore cannot be the reason for agreement, or lack of thereof, between the TIPIS and the experiment. In addition, the TDSE calculations [14] clearly supported the set of experimental angular offset values obtained with the use of nonadiabatic calibration of the field intensity [20]. In the meantime, the TIPIS simulations agreed with the adiabatic set of experimental data.

Implementation of the DKR model is very simple and transparent. It allows for some analytic derivations, in particular, an expression for the angular offset of the mean photoelectron momentum. Predictions of DKR agree well with numerical TDSE results for the He atom, similarly to the TIPIS without account for the polarization. However, the DKR model loses its accuracy for hydrogen because of a relatively strong Coulomb field experienced by the photoelectron at the exit from the tunnel.

The rest of the paper is organized according to the following plan. In Sec. II, we give a brief account of our TDSE technique and define the main observables such as the mean (central) photoelectron momentum, its angular dependence, and the positions of the angular extrema that define the attoclock offset angle $\theta_a$. In Sec. III, we describe our numerical DKR approach by formulating the set of initial conditions on the photoelectron position and velocity and feeding them to the Newton's classical equation of motion. Some analytic derivations for the DKR model are carried out in Sec. IV. Our numerical and analytic DKR results are validated against the TDSE in Sec. V. We conclude in Sec. VI by pointing to the weaknesses of the DKR model and looking for possible ways to strengthen it.

## II. TDSE MODEL

We solve the TDSE for the hydrogen and helium atoms driven by an elliptically polarized laser pulse. To isolate the effect of the Coulomb field of the ionic core, we also consider the model Yukawa atom. In this atom, the Coulomb field is screened while maintaining the same binding energy as in the hydrogen atom. The vector potential of the driving pulse is represented by

$$\boldsymbol{A}(t) = \frac{A_0}{\sqrt{\epsilon^2+1}} \cos^4(\omega t/2N) \begin{bmatrix} \epsilon \cos(\omega t)\, \epsilon_x \\ \sin(\omega t)\, \epsilon_y \end{bmatrix}, \qquad (1)$$

with the ellipticity parameter $\epsilon$ and the angular frequency $\omega$. The pulse length is parametrized with the number of optical cycles, $N$, and $\boldsymbol{A}$ vanishes for $|t| \geqslant N\pi/\omega$. In our simulations, we consider either a short circularly polarized pulse with

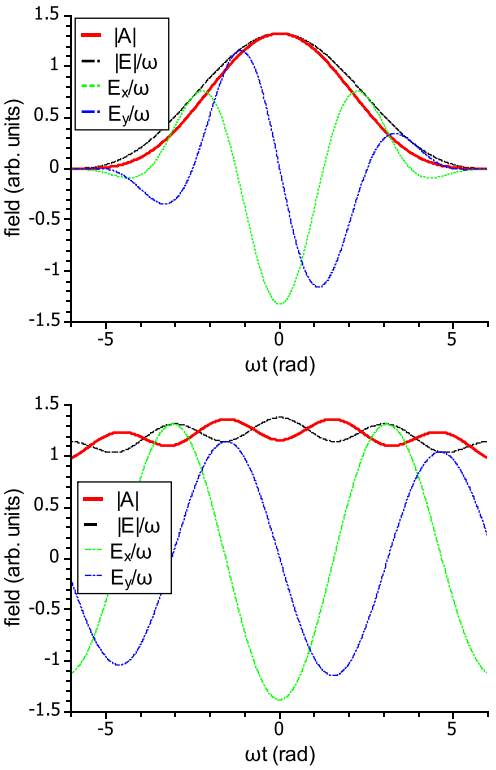


FIG. 1. The electrical field strength and the absolute value of the vector potential of the laser field. A short circularly polarized pulse (top) and a long elliptical polarized pulse with the ellipticity $\epsilon = 0.84$ (bottom).

$N = 2, \epsilon = 1$ or a long elliptical polarized pulse with $N = 10$, $\epsilon \lesssim 1$ (see Fig. 1 for graphical illustration). The latter pulse corresponds to typical pulse parameters used in experiments, while the former was used in the so-called numerical attoclock [11]. These two pulse types were previously used to calculate the attoclock offset angle and gave approximately the same results for it, while the use of the first type of pulses made it possible to save computer time considerably. However, for the momentum extremum offset angle, as we will show below, the results of these types of impulses are fundamentally different. With both kinds of driving pulses, the TDSE was solved by the split-operator method [21].

The PMD is projected onto the polarization plane $P(k_x, k_y, k_z = 0)$ and converted to the polar coordinates $P(k, \theta)$, where

$$k = \left(k_x^2 + k_y^2\right)^{1/2}, \ \theta = \tan^{-1}(k_y/k_x), \ 0 \leqslant \theta \leqslant \pi. \qquad (2)$$

In these coordinates, we define the directional probability of the photoelectron emission,

$$P(\theta) = \int dk\, P(k, \theta), \qquad (3)$$

and the mean (central) radial momentum in the given direction,

$$k_c(\theta) = \int kP(k, \theta)dk/P(\theta). \qquad (4)$$

The integration weight in Eqs. (3) and (4) corresponds to integration over a radially oriented narrow column of constant

TABLE I. Offset angle definitions.

| Notation | Meaning | Acronym |
|---|---|---|
| $\theta_a$ | Attoclock offset angle | AOA |
| $\theta_k$ | Momentum extremum offset angle | MEOA |
| $\Delta\theta$ | Coulomb field rotation angle | CFRA |

thickness starting at $k = 0$. An alternative is integration over a circular sector (weight $k$) or a spherical segment (weight $k^2$). However, the difference in all these options is small, so we used the first option everywhere.

Finally, the position of the angular maximum is found,

$$P(\theta_a) = \max P(\theta). \tag{5}$$

The angular maximum $\theta_a$ counted from the minor polarization axis defines the attoclock offset angle (AOA).

In addition, we calculate the momentum extremum offset angle (MEOA), which satisfies the following relation:

$$k_c(\theta_k) = \begin{cases} \min k_c(\theta), & \text{long pulse;} \\ \max k_c(\theta), & \text{short pulse with } \epsilon = 1. \end{cases} \tag{6}$$

Various definitions of the MEOA are used for short and long pulses for the following reason. In a long elliptic pulse, the peak electric field corresponds to the minimum vector potential, while in a short pulse, the vector potential at this instant is at its maximum (see Fig. 1).

In Sec. III, we also introduce the Coulomb field rotation angle (CFRA). This angle is not defined in TDSE and can only be determined in DKR. For convenience, we summarize all three definitions of the offset angles in Table I. In the conventional KR model, $\theta_k = \theta_a = \Delta\theta$. The identity $\theta_a = \Delta\theta$ follows from the basic premise of the KR in which the angular offset of the ionization probability is caused by the Coulomb scattering, while the shape of the angular distribution is not affected. As will be shown in Sec. IV B, there is a significant distortion of this distribution due to the phase volume change during the post-tunneling photoelectron motion. This leads to deviation of $\theta_a$ from $\Delta\theta$. The identity of $\theta_k = \Delta\theta$ in the KR follows from the elasticity of the Coulomb scattering which preserves the photoelectron momentum modulus. Hence, the angular offset of the photoelectron momentum is the same as the offset of the ionization probability. In reality, and as follows from the numerical solution of the TDSE, the angles $\theta_k$ and $\theta_a$ differ significantly, not only in magnitude but also in their signs. This strong qualitative effect is explained in DKR.

## III. NUMERICAL DKR MODEL

We subject an atom to a laser pulse with a vector potential,

$$\begin{aligned} A_x(t) &= -A_{x0} f(t) \cos\omega t, \\ A_y(t) &= +A_{y0} f(t) \sin\omega t, \\ A_z(t) &= 0. \end{aligned} \tag{7}$$

Here the envelope function $f(0) = 1$, $f(t \to \infty) = 0$ and the vector potential magnitudes,

$$A_{x0} = \epsilon A_0/\sqrt{1+\epsilon^2} < A_{y0} = A_0/\sqrt{1+\epsilon^2}, \tag{8}$$

define an elliptic polarization in the $(xy)$ plane. The attoclock offset angle $\theta_a$ is read relative to the minor polarization $y$ axis. The electric field vector is determined as

$$\boldsymbol{E}(t) = \partial \boldsymbol{A}(t)/\partial t. \tag{9}$$

We write the initial conditions under the assumption that the exit from the tunnel is in the direction of the laser electric field at the instant of tunneling and the longitudinal velocity at the exit point is zero,

$$\begin{aligned} \boldsymbol{r}_0 &= r_0 \boldsymbol{n}_E(t_0), \\ \boldsymbol{v}_0 &= (k_i + p_p)\boldsymbol{n}_p(t_0) + p_z \boldsymbol{n}_z. \end{aligned} \tag{10}$$

Here, $t_0$ is the time of the electron exit from the tunnel, $\boldsymbol{n}_E(t) = \boldsymbol{E}(t)/E(t)$ is the instantaneous electric field vector, and $\boldsymbol{n}_p(t)$ is a vector in the plane of polarization, perpendicular to the direction of the field, $[\boldsymbol{n}_p(t) \cdot \boldsymbol{n}_E(t)] = 0$, and directed approximately against the direction of the vector potential, i.e., $[\boldsymbol{n}_p(t) \cdot \boldsymbol{n}_A(t)] < 0$, where $\boldsymbol{n}_A(t) = \boldsymbol{A}(t)/A(t)$. Also defined is a vector perpendicular to the plane of polarization, $\boldsymbol{n}_z(t) = (0, 0, 1)$. An additional initial momentum $\boldsymbol{p}_\perp = (p_p \boldsymbol{n}_p, p_z)$ is introduced to account for the momentum spread (see Sec. IV C for more details).

The coordinate of the exit point is determined by the tunneling width given by Eq. (63) of Perelomov *et al.* [22] in the limit $\gamma \ll 1$:

$$r_0 = \frac{I_p + p_\perp^2/2}{E(t_0)}[1 - (1/4 - \epsilon^2/9)\gamma^2(t_0)]. \tag{11}$$

However, unlike the original work [22], we substitute the static Keldysh parameter $\gamma = \omega\kappa/E_{\max}$ with its dynamic equivalent $\gamma(t) = \omega\kappa/E(t)$. Here and throughout, $\kappa = \sqrt{2I_p}$ is the mean momentum of the bound electron. The photoelectron initial velocity $\boldsymbol{v}_0$ (10) contains the photoelectron momentum at the tunnel exit determined according to [22] in the same limit $\gamma \ll 1$ as

$$k_i = A(t_0)\gamma^2(t_0)/6 + O(\gamma^4). \tag{12}$$

We note that $\boldsymbol{v}_0$ is a dynamic quantity which depends on the electric field strength at the instant of tunneling. The parameters $p_p$ and $p_z$ are introduced via $\boldsymbol{p}_\perp$ to account for the photoelectron distribution in the radial and cylindrical directions.

The initial conditions (10) are fed into the Newton's equation of motion,

$$\ddot{\boldsymbol{r}} = -\frac{Z\boldsymbol{r}}{r^3} + \boldsymbol{E}(t), \tag{13}$$

which is solved for a set of initial times $t_0 = \phi/\omega$, where parameter $\phi$ was in the range from $-90^\circ$ to $+90^\circ$ with a step of $1^\circ$. From each solution, we determine the photoelectron exit angle $\theta = -\tan^{-1} k_y/k_x$ and the corresponding final momentum magnitude $k = \sqrt{k_x^2 + k_y^2}$. Here, $\boldsymbol{k} = \dot{\boldsymbol{r}}(t_{\text{fin}})$, and $t_{\text{fin}}$ is selected sufficiently large such that both the laser and the Coulomb fields are weak enough and can be neglected. From the exit angle $\theta$, we find the Coulomb field rotation angle (CFRA) $\Delta\theta = \theta(t_0 = 0)$ for the electrons emitted at the peak values of the electric field.

## IV. ANALyTIC DKR MODEL

### A. Angular shift of the central momentum extrema

We derive an analytic expression for the angular shift of the central momentum extrema due to the Coulomb field of the residual ion. We suppose that the photoelectron departs from the nucleus starting from the initial distance $r_0$. We also assume that most of the photoelectron momentum change due to the Coulomb field occurs before the distance from the nucleus is not very large. We quantify it by the time of travel, $t_1$, during which the distance to the nucleus doubles to $2r_0$.

*a. Strong field limit.* In the strong laser field limit, the photoelectron is accelerated very fast such that $t_1 \ll 1/\omega$. In this limit, the electric field of the laser pulse, $\boldsymbol{E}(t)$, can be considered constant before $r \gg r_0$. Thus,

$$t_1 = \sqrt{2r_0/E(t_0)} \simeq \kappa/E(t_0),$$

where we note that $r_0 \simeq I_p/E(t_0)$. The Coulomb force during this time interval is of the order of $\sim 1/r_0^2$ and directed approximately in the direction opposite to $\boldsymbol{E}(t_0)$. This force will impart the momentum

$$\boldsymbol{q}_E \sim -\frac{\boldsymbol{n}_E(t_0)}{r_0^2} t_1 \sim \frac{\boldsymbol{E}(t_0)}{\kappa^3}. \tag{14}$$

A more accurate estimate returns

$$\begin{aligned} \boldsymbol{q}_E &= -\boldsymbol{n}_E(t_0) \int_0^\infty \frac{Z}{[r_0 + E(t_0)t^2/2]^2} dt \\ &= -\frac{\pi Z}{\sqrt{8 r_0^3 E(t_0)}} \boldsymbol{n}_E(t_0) = -\frac{\pi Z}{\xi^{3/2}\kappa^3} \boldsymbol{E}(t_0). \end{aligned} \tag{15}$$

Here we set $r_0 = \xi I_p/E(t_0)$, where the coefficient $\xi$ is introduced to account for the difference between the true $r_0$ and its Keldysh model estimate $I_p/E(t_0)$.

At the instant $t_0 = 0$, the vector $\boldsymbol{q}_E$ is orthogonal to $\boldsymbol{A}$ and thus makes the strongest contribution to the photoelectron rotation angle due to the Coulomb field,

$$\Delta\theta \simeq \left.\frac{q_E}{A}\right|_{t_0=0} \sim \frac{\omega}{\epsilon\kappa^3}.$$

Here we noted that $E(0) = \omega A(0)/\epsilon$. This means that in the DKR model, $\Delta\theta$ tends to a constant in the limit of large laser field intensity. This is very different from the KR model in which $\Delta\theta \sim 1/A(0)$ and tends to zero in this limit.

Let us estimate the correction due to a finite initial velocity of the photoelectron. Because $\boldsymbol{k}_i \perp \boldsymbol{E}$, the photoelectron trajectory deviates from the radial direction by acquiring an additional momentum,

$$\boldsymbol{q}_p \sim -\frac{\boldsymbol{n}_p(t_0)}{r_0^3} k_i t_1^2 \sim \boldsymbol{n}_p(t_0) \frac{E(t_0)}{\kappa^4} k_i \sim (\omega/\kappa^2)\boldsymbol{n}_p(t_0).$$

A more accurate estimate at a small $k_i$ leads to

$$\begin{aligned} \boldsymbol{q}_E &= -\boldsymbol{n}_p(t_0) \int_0^\infty \frac{Z k_i t}{(r_0 + E(t_0)t^2/2)^2} dt \\ &= -\frac{Z k_i}{2 r_0^2 E(t_0)} \boldsymbol{n}_p(t_0) = -\frac{2 Z k_i E(t_0)}{\xi^2 \kappa^4} \boldsymbol{n}_p(t_0). \end{aligned} \tag{16}$$

Because $\boldsymbol{n}_p \parallel \boldsymbol{A}$ at $t_0 = 0$, the Coulomb field rotation angle (CFRA) can be approximated by

$$\Delta\theta = \tan^{-1} \left.\frac{q_E}{A + k_i + q_p}\right|_{t_0=0}. \tag{17}$$

As $k_i$ decreases with a growing laser intensity and $q_p$ tends to a constant, CFRA is also approaching a constant value given by the above expression.

Now we estimate the angular direction of the momentum maximum. For convenience, we convert the instant of tunneling to an angular variable $\phi = \omega t_0$. We also introduce

$$\boldsymbol{q}_E = -a\boldsymbol{A}'(\phi), \quad \boldsymbol{q}_p = -b\boldsymbol{n}_p(\phi), \quad \boldsymbol{k}_i = c\frac{A(\phi)}{|A'(\phi)|^2}\boldsymbol{n}_p(\phi), \tag{18}$$

where $\boldsymbol{A}'(\phi) = \boldsymbol{E}(t_0)/\omega$ and $a$, $b$, and $c$ are constants:

$$a = \frac{\pi Z \omega}{\xi^{3/2}\kappa^3}, \quad b = \frac{2Z\epsilon\omega}{\xi^2\kappa^4} c, \quad c = \frac{\kappa^2}{6}. \tag{19}$$

In these notations, the CFRA

$$\Delta\theta = \tan^{-1} \frac{a}{\epsilon} \left[1 + \frac{k_i - b}{A}\right]^{-1}\Bigg|_{\phi=0}. \tag{20}$$

The total final momentum becomes $\boldsymbol{k} = -\boldsymbol{A} + \boldsymbol{k}_i + \boldsymbol{q}_E + \boldsymbol{q}_p$ and its modulus squared is

$$\begin{aligned} k^2(\phi) = A^2 + a^2|\boldsymbol{A}'|^2 + (k_i - b)^2 \\ + 2a(\boldsymbol{A}\cdot\boldsymbol{A}') - 2(k_i - b)(\boldsymbol{A}\cdot\boldsymbol{n}_p). \end{aligned} \tag{21}$$

At the instant of tunneling $t_i = 0$, the vector potential and the electric field strength are at their peak values and their directions are orthogonal,

$$\begin{aligned} A'(0) = 0; \quad |\boldsymbol{A}'|'(\phi = 0) = 0; \\ (\boldsymbol{A}\cdot\boldsymbol{A}')|_{\phi=0} = 0; \quad (\boldsymbol{A}\cdot\boldsymbol{n}_p)|_{\phi=0} = -A(0). \end{aligned} \tag{22}$$

We also note that $|\boldsymbol{A}'(0)| = A(0)/\epsilon$ and, for a long pulse, $\boldsymbol{A}''(0) \simeq -\boldsymbol{A}(0)$.

We make a Taylor expansion of $k^2(\phi)$ near $\phi = 0$, keep the terms up to the second order in $\phi$, and neglect the squares of the small quantities $k_i$, $a$, and $b$. In this way, we obtain

$$\begin{aligned} k^2(\phi) = A(0)^2 + 2(k_i - b)A(0) + 2a\,(\boldsymbol{A}\cdot\boldsymbol{A}')'|_{\phi=0}\phi \\ + [(A^2)''(0) + [2(k_i - b)A]''|_{\phi=0}]\frac{\phi^2}{2}. \end{aligned} \tag{23}$$

Hence we find the angular maximum of $k^2(\phi)$,

$$\begin{aligned} \phi_k &= -a\left\{P1 - \frac{2[(k_i - b)A]''}{(A^2)''}\right\}^{-1}\Bigg|_{\phi=0} \\ &= -a\left[1 + \frac{(k_i - b)}{A} + \frac{2k_i'' A}{(A^2)''}\right]^{-1}\Bigg|_{\phi=0}. \end{aligned} \tag{24}$$

This maximum corresponds to the momentum extremum offset angle (MEOA),

$$\theta_k = \theta_A(\phi_k) + \Delta\theta \simeq \left.\frac{a}{\epsilon}\frac{k_i''}{A''}\right|_{\phi=0} = ac\epsilon \left.\frac{1 - 2\epsilon\nu}{A^2}\right|_{\phi=0}, \tag{25}$$

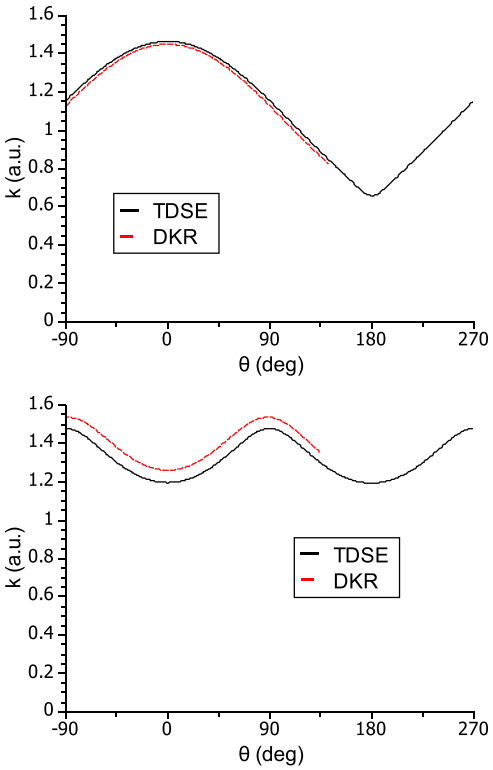


FIG. 2. The central photoelectron radial momentum $k_c$ as a function of the exit angle $\theta$ for the Yukawa atom. A short circular pulse (top) and a long elliptic pulse with the ellipticity $\epsilon = 0.84$ (bottom). Both pulses correspond to the field intensity of $4 \times 10^{14}$ W/cm$^2$.

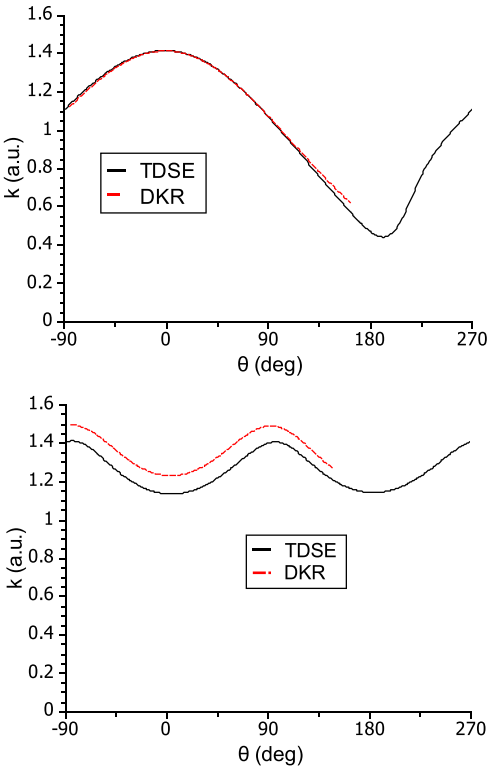


FIG. 3. Same as Fig. 2 for the hydrogen atom.

where

$$\nu = \left.\frac{|\boldsymbol{A}'|''}{A''}\right|_{\phi=0} = \left.\frac{E''}{\omega A''}\right|_{\phi=0} = \begin{cases} -\epsilon, & \text{long pulse;} \\ 1 + f''(0)/f(0)/\omega^2, & \text{short pulse with } \epsilon = 1. \end{cases} \quad (26)$$

We see that $\theta_k > 0$ for a long pulse with $\epsilon \lesssim 1$, while $\theta_k < 0$ for a short circular pulse with $\epsilon = 1$. In both cases, $\theta_k$ is inversely proportional to the field intensity. Also, as $a \simeq \epsilon \Delta\theta$, $|\theta_k| \ll \Delta\theta$ when $A^2 \gg \kappa^2/6$ in the case of high laser pulse intensities.

*b. Weak field limit.* In the opposite limit of a very weak field intensity, the photoelectron gains its momentum from the laser pulse in the vicinity of the point of the closest approach to the Coulomb center. Hence the conventional KR model applies to this case. The photoelectron scattering on the Coulomb field changes its direction without any significant change of the radial momentum. Thus, in this limit, $\theta_a \simeq \Delta\theta$.

### B. Ionization probability angular distribution

We assume that the instantaneous ionization rate is determined by a static field with the strength equal to that of the laser field at the instant of tunneling, $E(t_0)$. According to Perelomov *et al.* [22], in the absence of the Coulomb field, this probability is proportional to

$$w_0(E, p_\perp) \sim \exp\left[-\frac{2}{3}\frac{\kappa^3}{E} - \frac{\kappa}{E}p_\perp^2\right]. \quad (27)$$

Here, $p_\perp$ is the transverse photoelectron momentum in the direction orthogonal to the polarization plane. This transverse momentum is distributed in the initial state wave function in the momentum space. In the case of the Coulomb field, an additional preexponential factor should be introduced [23],

$$w(E, p_\perp) \sim \left(\frac{2\kappa'^3}{E}\right)^{2Z/\kappa} w_0(E, p_\perp). \quad (28)$$

Here, $\kappa' = \sqrt{\kappa^2 + p_\perp^2}$ and $Z$ is the charge of the residual ion. Note that expression (28) is a combination of two different formulas. In the preexponential factor, which is sourced from [23], $\kappa$ is replaced with $\kappa'$, similarly to the derivation of Eq. (27) in [23].

As previously, we convert $t_0$ to an angular variable $\phi = \omega t_0$ and define $w(\phi) \equiv w[E(t_0), 0]$. We assume that the photoelectron exits the tunnel at the coordinate $\boldsymbol{r}_0$ when the electric field vector $\boldsymbol{E}$ points to the direction defined by the angular interval $d\theta_E$. The ionization probability is proportional to the time during which the $\boldsymbol{E}$ vector remains in this angular interval, $dt = d\theta_E (d\theta_E/dt)^{-1}$. By noting that $dt_0 = \phi/\omega$, the probability of emitting the photoelectron in the unit volume of the initial momentum space $dp_p d\phi dp_z$ is

$$dP \sim w(\phi)\left[\frac{d\theta_E}{dt}\right]^{-1} dp_p d\phi dp_z.$$

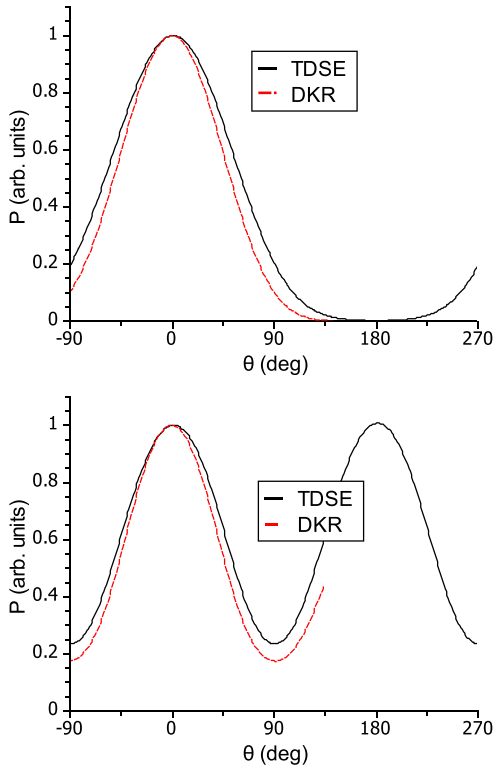


FIG. 4. Directional probability of the photoelectron emission $P(\theta)$ for the Yukawa atom. The same pulse parameters as in Figs. 2 and 3: a short circular pulse (top) and a long elliptical pulse with $\epsilon = 0.84$ (bottom).

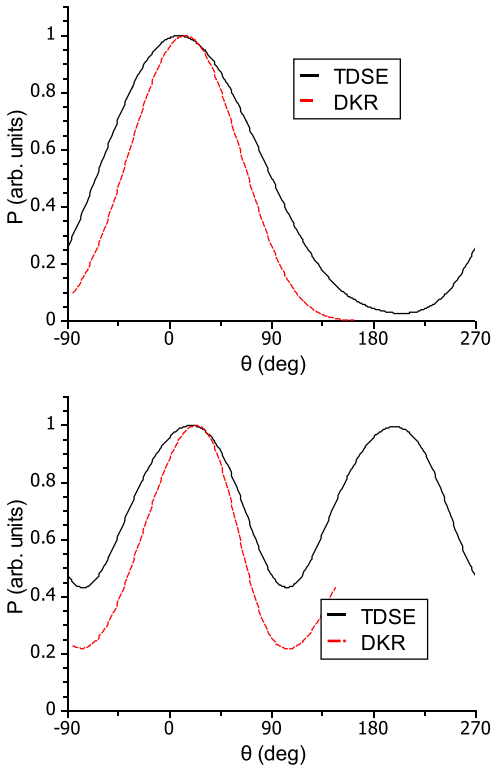


FIG. 5. Same as in Fig. 4 for the hydrogen atom.

The corresponding probability of finding the photoelectron in the unit volume of the final momentum space $dkd\theta dk_z$ is

$$d^3P = \frac{d^3P}{dkd\theta dk_z} dkd\theta dk_z = \frac{d^3P}{dkd\theta dk_z} J dp_p d\phi dp_z.$$

Here we introduce a Jacobian,

$$J = \begin{vmatrix} \frac{\partial k}{\partial p_p} & \frac{\partial \theta}{\partial p_p} & \frac{\partial k_z}{\partial p_p} \\ \frac{\partial k}{\partial \phi} & \frac{\partial \theta}{\partial \phi} & \frac{\partial k_z}{\partial \phi} \\ \frac{\partial k}{\partial p_z} & \frac{\partial \theta}{\partial p_z} & \frac{\partial k_z}{\partial p_z} \end{vmatrix}.$$

This leads us to

$$\frac{d^3P}{dkd\theta dk_z} \sim \left[ J \frac{d\theta_E}{dt} \right]^{-1} w[\phi(\theta)]. \tag{29}$$

In the above expression, $\phi = \phi(\theta)$ is the inverse function connecting the instant of tunneling $t_0$ with the photoelectron direction. The dominant contribution to the Jacobian is given by its diagonal terms, $J \simeq \frac{\partial k}{\partial p_r} \frac{\partial \theta}{\partial \phi} \frac{\partial k_z}{\partial p_z}$. In the absence of the Coulomb field $Z = 0$, the derivative $\frac{\partial k_z}{\partial p_z} = 1$, while the time derivative of the angle is found in the Appendix. The angle itself can be approximated as

$$\theta(\phi) = \theta_A(\phi) + \Delta\theta(\phi), \tag{30}$$

where $\theta_A(\phi)$ is the emission angle in the absence of the Coulomb field and the zero initial velocity (see the Appendix), and $\Delta\theta(\phi)$ is the photoelectron rotation angle due to the Coulomb field. The attoclock offset angle $\theta_a$ will coincide with the Coulomb rotation angle $\Delta\theta(0)$, while the angular distribution will be Gaussian if, and only if, $[J \frac{d\theta_E}{dt}]^{-1} = \text{const}$.

### C. The root-mean-square momentum deviation

Besides the central photoelectron momentum $k_c$, the root-mean-square deviation $D(\theta) = \overline{(k - k_c)^2}$ can also be extracted from the photoelectron momentum distribution. It can be calculated by assuming that the initial longitudinal momentum spread $\boldsymbol{p}_\perp$ satisfies Eq. (27). Note that in the case of a close-to-circular polarization, the component $\boldsymbol{p}_\perp$ in the plane of polarization $p_p \boldsymbol{n}_p$ is directed approximately parallel to $\boldsymbol{A}$, and thus the spread in the values of $p_p$ leads to the scatter in the radial component of the final momentum.

Equation (27) can be rewritten as $w_0[E(t_0), p_\perp] \sim \exp[-(p_\perp/\Delta p)^2]$, where the width of the distribution over $p_p$ is

$$\Delta p(\phi) = \sqrt{\frac{E(t_0)}{\kappa}} = \sqrt{\frac{\omega}{\gamma(t_0)}}. \tag{31}$$

In the presence of a Coulomb field, due to the dependence on $p_p$ of the preexponential factor in Eq. (28), the width becomes somewhat larger,

$$\Delta p(\phi) = \left[ \frac{\kappa}{E(t_0)} - \frac{3Z}{\kappa^3} \right]^{-1/2}. \tag{32}$$

Suppose that the distribution over the final radial momentum is $P(k) \sim \exp[-(k/\Delta k)^2]$ and there is a one-to-one corre-

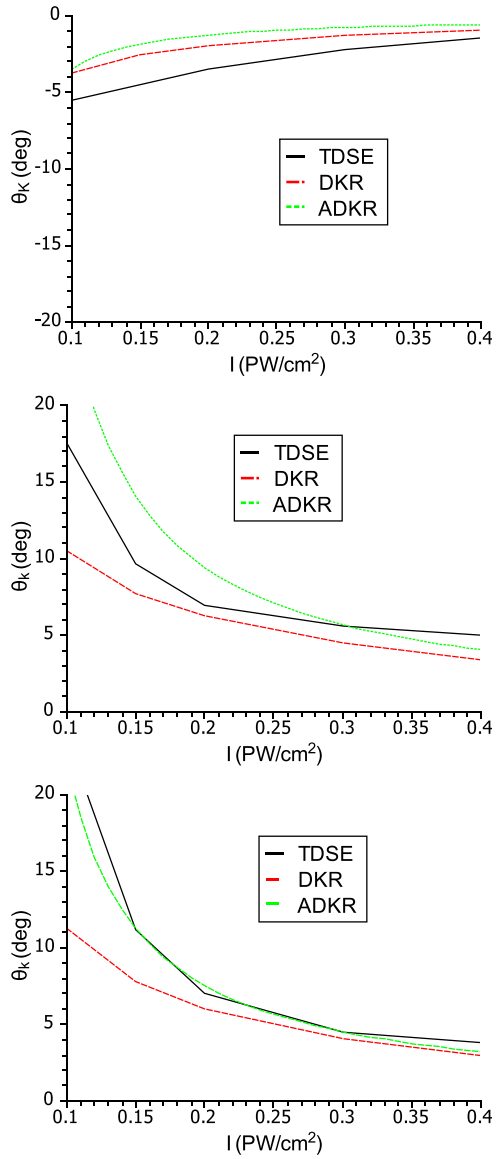


FIG. 6. The angular maximum rotation angle $\theta_k$ as a function of the field intensity for the hydrogen atom. A short circular pulse (top) and a long elliptical pulse with $\epsilon = 0.95$ (middle) and $\epsilon = 0.84$ (bottom). The field intensity scale is in units of PW/cm$^2$ = $1 \times 10^{15}$ W/cm$^2$.

spondence $p \leftrightarrow k$. In this case, if we calculate the finite radial momenta $k_\pm$ with initial conditions $p_p = \pm\eta\Delta p$, then $\Delta k$ can be expressed as $\Delta k = (k_+ - k_-)/2\eta$. Taking into account the assumed Gaussian distribution of the final photoelectron momentum, we obtain

$$D(\theta) = \frac{(\Delta k)^2}{2} = \frac{[k_+(\theta) - k_-(\theta)]^2}{8\eta}. \tag{33}$$

In the calculations below, we assume $\eta = 1/\sqrt{2}$ so that $k_\pm$ corresponds to momenta at which the emission probability is equal to $\exp(-1/2)$ of the maximum corresponding to $k_c$.

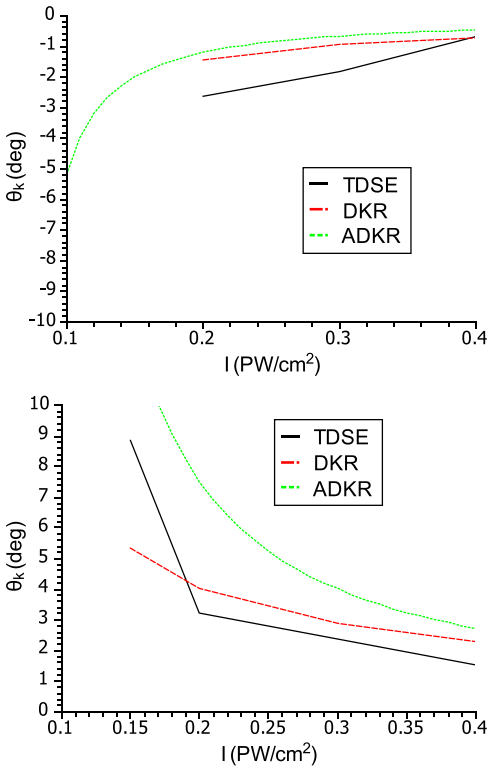


FIG. 7. Same as Fig. 6 for the He atom. A short circular pulse (top) and a long elliptical pulse with $\epsilon = 0.84$ (bottom).

## V. VALIDATION OF THE DKR MODEL

We start validating our DKR model against the TDSE results by evaluating the central photoelectron momentum in the radial direction $k_c$. This momentum is determined according to Eq. (4) in TDSE. In DKR, it corresponds to the zero initial transverse momentum $p_\perp = 0$. Results of this comparison are presented in Figs. 2 and 3 for the Yukawa and hydrogen atoms, respectively. Here the central radial momentum is plotted in various photoelectron emission directions.

The two pulse durations $T = NT_{\rm opt}$ are considered. The first case is a very short circular pulse with $N = 2$ and the photon energy $\omega = 1.55$ eV $= 0.057$ a.u. (the wavelength 800 nm). The second case is a moderately long elliptical pulse with $N = 10$ and carrier frequency $\omega = 1.61$ eV$= 0.0592$ a.u. (wavelength 770 nm). These pulses are taken at the field intensity of $4 \times 10^{14}$ W/cm$^2$ corresponding to the Keldysh parameter $\gamma = 0.7$. For the short circular pulse, there is a nearly perfect agreement between the DKR and TDSE. For a longer pulse with a larger ellipticity, $\epsilon = 0.84$, the DKR results slightly exceed that of the TDSE. This can be explained by the fact that the present version of DKR assumes that ionization occurs only during the period with the maximum amplitude, near the center of the pulse. In fact, periods with lower field intensity also make a significant contribution, due to which the real average momentum is slightly lower.

Figure 4 displays the directional probability of the photoelectron emission $P(\theta)$ given by Eq. (3) for the Yukawa atom. In all cases, agreement of the TDSE and DKR results is good. An analogous set of the hydrogen data is displayed in Fig. 5. The agreement between the DKR and TDSE is

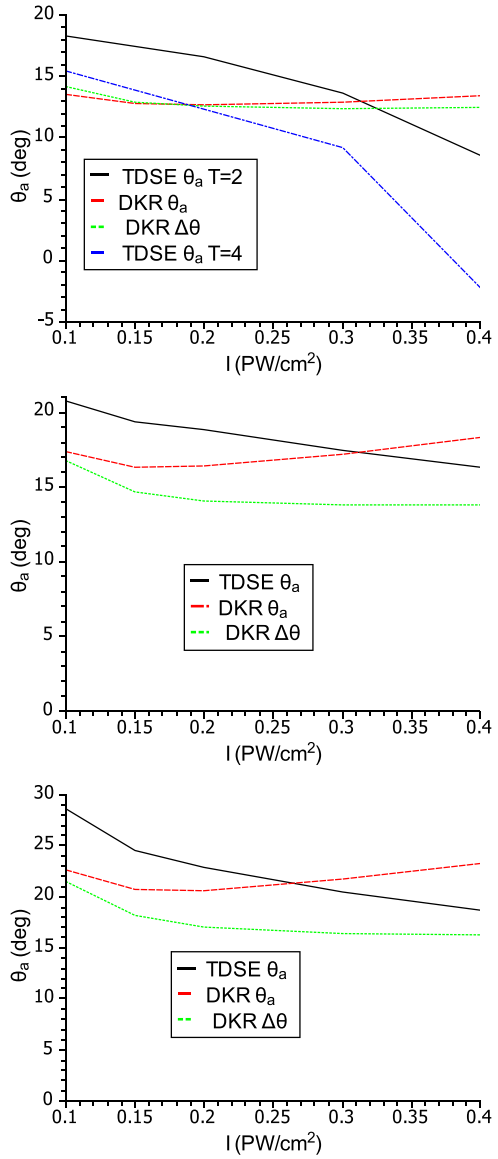


FIG. 8. The attoclock offset angle $\theta_a$ as a function of the field intensity for the hydrogen atom. A short circular pulse (top) and a long pulse with $\epsilon = 0.95$ (middle) and $\epsilon = 0.84$ (bottom).

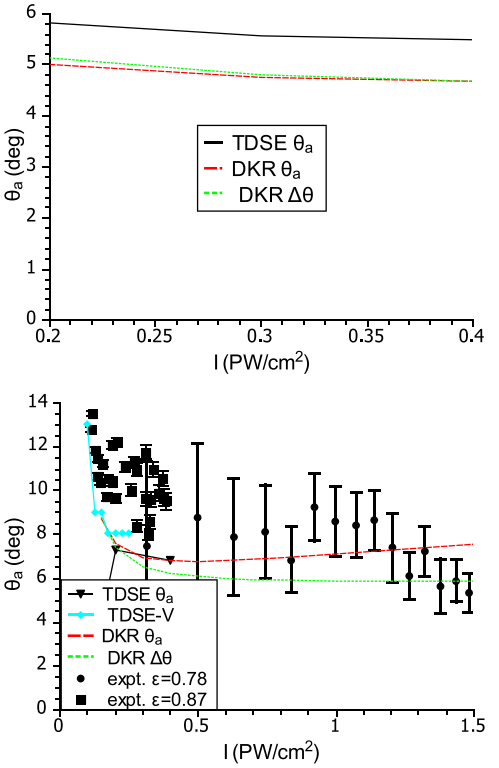


FIG. 9. Same as Fig. 8 for the helium atom. A short circular pulse (top) and a long elliptical pulse with $\epsilon = 0.84$ (bottom). Experimental data for $\epsilon = 0.78$ [3] and $\epsilon = 0.87$ [20], and theoretical results TDSE-V from [14], are also shown.

significantly worse than for the Yukawa atom. The angular width is substantially smaller and the attoclock offset angle $\theta_a$ is larger than that in the TDSE.

Figures 6 and 7 display the angular maximum rotation angle $\theta_k$ as a function of the laser field intensity for the H and He atoms, respectively. Both the numerical DKR and analytic DKR (ADKR) results returned by Eq. (25) are compared with the TDSE. In the case of He, the TDSE with SAE approximation was used for calculations marked as TDSE. We see that the prediction of the opposite signs of $\theta_k$ for a short circular and long elliptical pulses is supported by both sets of calculations. At a large field intensity, a good quantitative agreement is also reached with the TDSE results. In the very low field intensity limit, tunneling ionization turns into a multiphoton process which is not expected to be reproduced by a classical model.

Figure 8 displays the attoclock offset angle $\theta_a$ as a function of the laser pulse intensity for the hydrogen atom. The TDSE results are compared with the DKR predictions. For the latter model, the photoelectron rotation angles in the field direction $\Delta\theta$ are also plotted. The DKR dependence is very different from that of the TDSE. Indeed, the attoclock offset angle $\theta_a$ is growing with the pulse intensity in the DKR, while it is falling in the TDSE. Meanwhile, the difference of $\theta_a$ and $\Delta\theta$ is of the same order in DKR as the difference between the DKR and TDSE. Thus, the effect of changing the volume element of the momentum space [which, in the present model, is described by the factor in square brackets in Eq. (29)] has a significant impact on the results of the DKR and its more accurate account may eventually improve this model.

Most troubling is the disagreement of the DKR and TDSE for a short pulse. To demonstrate that $\theta_a \neq \Delta\theta$ in this case, we carried out yet another TDSE calculation for a longer $N = 4$ circular pulse. As seen in Fig. 8 (top), this doubling of the pulse duration reduced the corresponding offset angles $\theta_a$. These angles turned negative at the top end of the intensity scale. Changing pulse duration does not change the peak vector potential and the electric field values. Thus it cannot change the photoelectron rotation angle $\Delta\theta$ either in the KR or the DKR model. This indicates the presence of another factor which affects the photoelectron angular distribution and which depends on the pulse duration, but is not accounted for

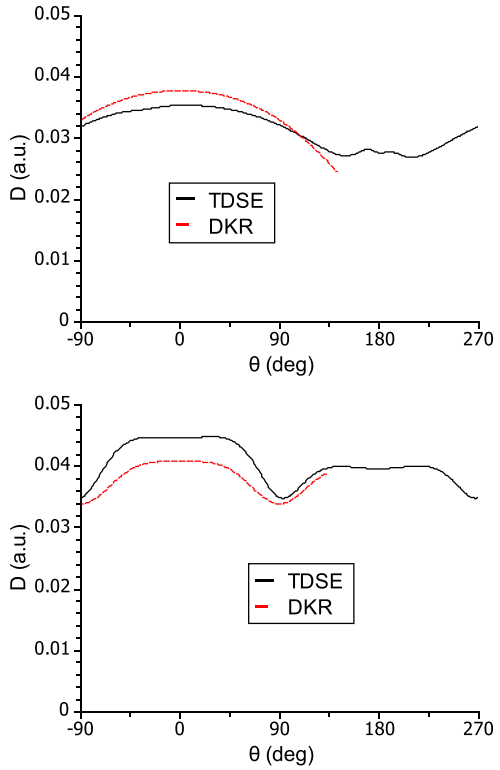


FIG. 10. Dependence of the root-mean-square deviation of the radial momentum on the emission angle for the Yukawa atom. A short circular pulse (top) and a long pulse with the polarization $\epsilon = 0.84$ (bottom).

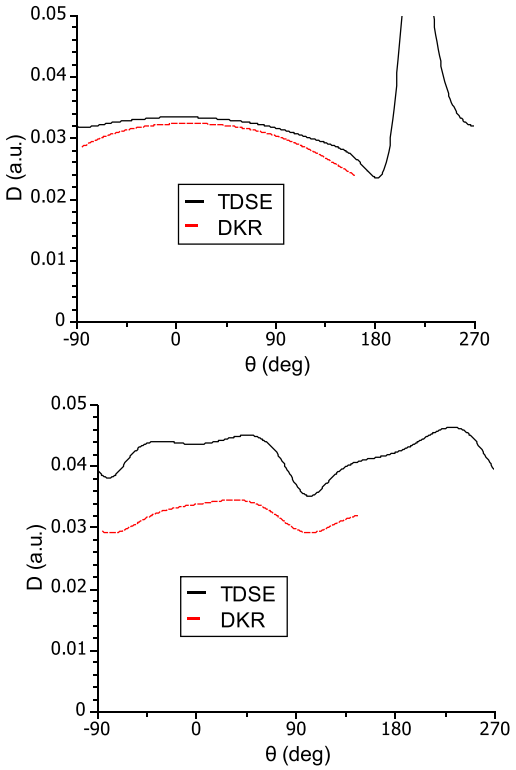


FIG. 11. Same as Fig. 10 for the hydrogen atom.

in Eq. (29). This factor emulates the Rutherford-like dependence of $\theta_a$ on the photoelectron momentum in the KR model.

Meanwhile, for the helium atom, Fig. 9 displays a very good agreement of the attoclock offset angles $\theta_a$ calculated by both the numerical and analytic DKR, the latter based on Eq. (29), with the TDSE. These values are close to the earlier TDSE calculations[14]. Most probably, such a good agreement for He is related to a larger ionization potential of the He atom and the correspondingly larger $r_0$ at the same field intensity. Hence, $\Delta\theta$ is small for He. We note that our $\theta_a$ values are close to the experiment and theoretical TIPIS results presented in [3].

We offer the following explanation of the difficulties of the present version of DKR when calculating $\theta_a$. This model fairly well predicts the mean momentum and MEOA $\theta_k$ in close agreement with TDSE. The photoelectron momentum is gained due to the combined action of the laser and Coulomb fields after leaving the classically forbidden region, while MEOA depends on the initial conditions at the exit point. This indicates that the initial conditions and the photoelectron trajectory after the tunneling are described rather accurately in our approach. We also notice that our account of the curvature of photoelectron trajectories after the tunneling due to the Coulomb field does not improve the agreement between DKR and TDSE for the angular probability distribution and, consequently, $\theta_a$. These observations lead us to believe that the source of the error lies in calculating the tunneling probability. Namely, the assumption that the instantaneous ionization rate is determined by a static field with the strength equal to that of the laser field at the instant of tunneling is not valid in the presence of the Coulomb field. From the results for He, we can conclude that the accuracy of the approximation of the instantaneous ionization rate improves with the increasing distance to the exit point $r_0$ and, accordingly, with the decreasing Coulomb field near it.

Finally, we display our results for the root-mean-square deviation of the radial momentum. For the Yukawa atom, as seen from Fig. 10, there is a good agreement between the results of the analytic DKR theory and the numerical TDSE results. In general, for the Yukawa atom, angular distributions of all values are well reproduced by theory.

However, for the hydrogen atom, as seen from Fig. 11, the agreement of the numerical and analytic results for $D$ is considerably worse, both in the shape and magnitude. Of particular note is a 25% underestimation of the analytic results for the case of $\epsilon = 0.84$, which is observed despite the fact that we took into account the increase in the momentum distribution width due to the presence of the preexponential factor. Without this factor taken into account, the difference from the TDSE results is generally almost twofold. As expected, with an enforced increase in $r_0$, the value of $D$ grows and its distribution approaches the distribution for the Yukawa atom. With an enforced increase in the initial velocity $k_i$, the asymmetry of the peak of the $D$ distribution increases. Thus, the distribution of $D$ can serve as an independent test for determining $r_0$ and $k_i$.

## VI. CONCLUSION

We have developed a dynamic extension of the Keldysh-Rutherford model. The DKR model takes the initial conditions from the Keldysh theory of tunneling ionization in the $\gamma \ll 1$ limit. These initial conditions are actually applicable to a wider range of tunneling conditions $\gamma \lesssim 1$ as was tested by the saddle-point method calculations [15]. We plug the initial $r_0$ and $k_i$ into the classical Newton' equation of motion for the photoelectron in the Coulomb field of the ionic core and the electric field of the driving laser pulse. This equation is solved numerically. Such a numerical DKR model correctly predicts the central radial momentum, its angular distribution, and the position of the angular extrema. In addition, an analytic DKR theory is developed. The model is based on the assumption of the straight motion and a uniform acceleration of the electron in the laser field in the region where the Coulomb force of the residual ion is sufficiently strong.

We attempted to extend the DKR model by driving it with the instantaneous ionization rate in a static field equated with the electric field of the laser pulse at the instant of tunneling. For the Yukawa and helium atoms, this extended DKR model works rather well. However, for the hydrogen atom, the angular distribution of the emission probabilities and the position of the angular extrema are poorly described. For the root-mean-square deviation of the radial momentum, the accuracy of this model for the hydrogen atom is also not entirely satisfactory.

Nevertheless, the mean photoelectron momentum, gained after the tunneling, is predicted by the DKR model rather well for all the considered targets. This points us to the tunneling stage, which presents the difficulty for the present DKR model. More specifically, the presence of a Coulomb field invalidates the assumption that the instantaneous ionization rate is determined by a static field with the strength equal to that of the laser field at the instant of tunneling. The Coulomb field distorts the angular emission pattern already at this early tunneling stage. For an enhanced DKR model, an improved expression for the ionization rate is required, taking into account both the time-dependent laser and static Coulomb fields. Such an expression can be derived using the saddle-point method. This extension goes beyond the scope of the present work and will be attempted in the future.

## APPENDIX: DIRECTIONS OF THE ELECTRIC FIELD AND THE VECTOR POTENTIAL

The direction of the vector potential $\boldsymbol{A}(t)$ is

$$\theta_A(t) = \tan^{-1}[\tan(\omega t)/\epsilon],$$
$$\frac{d\theta_A}{dt} = \omega \frac{\epsilon}{(\epsilon^2-1)\cos^2\omega t + 1} = \omega[\epsilon^2 + (1-\epsilon^2)\cos^2\theta_A]/\epsilon. \quad \text{(A1)}$$

Hence, the dependence of the absolute value of the momentum of the emitted electron on the angle (counted from the direction of the most probable ejection in the absence of a long-range field) is

$$|k_0(\theta)|^2 = k_{\min}^2 \frac{1}{(1-\epsilon^2)\cos^2\theta + \epsilon^2}. \quad \text{(A2)}$$

The direction of the electric field vector $\boldsymbol{E}(t) = d\boldsymbol{A}(t)/dt$ (neglecting the derivative of the envelope) is

$$\theta_E(t) = -\tan^{-1}[\cot(\omega t)/\epsilon], \quad \text{(A3)}$$

$$\frac{d\theta_E}{dt} = \omega \frac{\epsilon}{(1-\epsilon^2)\cos^2\omega t + \epsilon^2}. \quad \text{(A4)}$$

From this, we obtain the relationship between the departure angle (in the absence of the nuclear field) and the direction of the electric field at the time of tunneling,

$$\theta_E = -\tan^{-1}[\cot\theta_A/\epsilon^2] = \tan^{-1}[\tan(\theta_A - \pi/2)/\epsilon^2]. \quad \text{(A5)}$$

In the case of a short circularly polarized laser pulse, the maximum strength modulus $E(t)$ and maximum $A(t)$ coincide in time. If we set $|\boldsymbol{A}(t)| = A_0 f(t)$, where $f(t)$ is the pulse envelope, then the direction of $\boldsymbol{A}(t)$ in this case is

$$\theta_A(t) = \omega t \quad \text{(A6)}$$

and

$$k_0(\theta) = f(\theta/\omega)k_{\max}. \quad \text{(A7)}$$

The direction of the electric field vector $\boldsymbol{E}(t) = d\boldsymbol{A}(t)/dt$, assuming the first derivative of the envelope to be small, is

$$\theta_E(t) = \omega t - \pi/2 - \frac{f'(t)}{\omega f(t)}. \quad \text{(A8)}$$


[1] P. Eckle, M. Smolarski, P. Schlup, J. Biegert, A. Staudte, M. Schoffler, H. G. Muller, R. Dorner, and U. Keller, Attosecond angular streaking, Nat. Phys. **4**, 565 (2008).

[2] P. Eckle, A. N. Pfeiffer, C. Cirelli, A. Staudte, R. Dorner, H. G. Muller, M. Buttiker, and U. Keller, Attosecond ionization and tunneling delay time measurements in helium, Science **322**, 1525 (2008).

[3] A. N. Pfeiffer, C. Cirelli, M. Smolarski, D. Dimitrovski, M. Abu-samha, L. B. Madsen, and U. Keller, Attoclock reveals natural coordinates of the laser-induced tunnelling current flow in atoms, Nat. Phys. **8**, 76 (2012).

[4] A. S. Landsman, M. Weger, J. Maurer, R. Boge, A. Ludwig, S. Heuser, C. Cirelli, L. Gallmann, and U. Keller, Ultrafast resolution of tunneling delay time, Optica **1**, 343 (2014).

[5] N. Camus, E. Yakaboylu, L. Fechner, M. Klaiber, M. Laux, Y. Mi, K. Z. Hatsagortsyan, T. Pfeifer, C. H. Keitel, and R. Moshammer, Experimental Evidence for Quantum Tunneling Time, Phys. Rev. Lett. **119**, 023201 (2017).

[6] U. S. Sainadh, H. Xu, X. Wang, A. Atia-Tul-Noor, W. C. Wallace, N. Douguet, A. Bray, I. Ivanov, K. Bartschat, A. Kheifets *et al.*, Attosecond angular streaking and tunnelling time in atomic hydrogen, Nature (London) **568**, 75 (2019).

[7] A. S. Kheifets, The attoclock and the tunneling time debate, J. Phys. B: At. Mol. Opt. Phys. **53**, 072001 (2020).

[8] U. S. Sainadh, R. T. Sang, and I. V. Litvinyuk, Attoclock and the quest for tunnelling time in strong-field physics, J. Phys. Photon. **2**, 042002 (2020).

[9] C. Hofmann, A. Bray, W. Koch, H. Ni, and N. I. Shvetsov-Shilovski, Quantum battles in attoscience: Tunneling, Eur. Phys. J. D **75**, 208 (2021).

[10] L. Torlina, F. Morales, J. Kaushal, I. Ivanov, A. Kheifets, A. Zielinski, A. Scrinzi, H. G. Muller, S. Sukiasyan, M. Ivanov *et al.*, Interpreting attoclock measurements of tunnelling times, Nat. Phys. **11**, 503 (2015).

[11] V. V. Serov, A. W. Bray, and A. S. Kheifets, Numerical attoclock on atomic and molecular hydrogen, Phys. Rev. A **99**, 063428 (2019).

[12] C. P. J. Martiny, M. Abu-samha, and L. B. Madsen, Counterintuitive angular shifts in the photoelectron momentum distribution for atoms in strong few-cycle circularly polarized laser pulses, J. Phys. B: At. Mol. Opt. Phys. **42**, 161001 (2009).

[13] I. Barth and M. Lein, Numerical verification of the theory of nonadiabatic tunnel ionization in strong circularly polarized laser fields, J. Phys. B: At. Mol. Opt. Phys. **47**, 204016 (2014).

[14] I. A. Ivanov and A. S. Kheifets, Strong-field ionization of He by elliptically polarized light in attoclock configuration, Phys. Rev. A **89**, 021402(R) (2014).

[15] V. V. Serov, J. Cesca, and A. S. Kheifets, Numerical and laboratory attoclock simulations on noble-gas atoms, Phys. Rev. A **103**, 023110 (2021).

[16] E. Yakaboylu, M. Klaiber, and K. Z. Hatsagortsyan, Wigner time delay for tunneling ionization via the electron propagator, Phys. Rev. A **90**, 012116 (2014).

[17] H. Ni, U. Saalmann, and J.-M. Rost, Tunneling Ionization Time Resolved by Backpropagation, Phys. Rev. Lett. **117**, 023002 (2016).

[18] J. Liu, Y. Fu, W. Chen, Z. Lü, J. Zhao, J. Yuan, and Z. Zhao, Offset angles of photocurrents generated in few-cycle circularly polarized laser fields, J. Phys. B: At. Mol. Opt. Phys. **50**, 055602 (2017).

[19] A. W. Bray, S. Eckart, and A. S. Kheifets, Keldysh-Rutherford Model for the Attoclock, Phys. Rev. Lett. **121**, 123201 (2018).

[20] R. Boge, C. Cirelli, A. S. Landsman, S. Heuser, A. Ludwig, J. Maurer, M. Weger, L. Gallmann, and U. Keller, Probing Nonadiabatic Effects in Strong-Field Tunnel Ionization, Phys. Rev. Lett. **111**, 103003 (2013).

[21] V. V. Serov, Calculation of intermediate-energy electron-impact ionization of molecular hydrogen and nitrogen using the paraxial approximation, Phys. Rev. A **84**, 062701 (2011).

[22] A. Perelomov, V. Popov, and M. Terent'ev, Ionization of atoms in an alternating electric field II, Sov. Phys. JETP **24**, 207 (1967).

[23] A. Perelomov, V. Popov, and V. P. Kuznetsov, Allowance for the Coulomb interaction in multiphoton ionization, Sov. Phys. JETP **27**, 451 (1968).